

NIH RELAIS Document Delivery

NIH-10286765

JEFFDUYN

NIH -- W1 MA34IF

JOZEF DUYN
10 Center Dirve
Bldg. 10/Rm.1L07
Bethesda, MD 20892-1150

ATTN: SUBMITTED: 2002-08-29 17:22:17
PHONE: 301-594-7305 PRINTED: 2002-09-03 07:35:16
FAX: - REQUEST NO.: NIH-10286765
E-MAIL: SENT VIA: LOAN DOC
7967419

NIH	Fiche to Paper	Journal
TITLE:	MAGNETIC RESONANCE IN MEDICINE : OFFICIAL JOURNAL OF THE SOCIETY OF MAGNETIC RESONANCE IN MEDICINE / SOCIETY OF MAGNETIC RESONANCE IN MEDICINE	
PUBLISHER/PLACE:	Wiley-Liss, Inc., a division of John Wil New York, NY :	
VOLUME/ISSUE/PAGES:	1995 Mar;33(3):439-42	439-42
DATE:	1995	
AUTHOR OF ARTICLE:	van Gelderen P; Moonen CT; Duyn JH	
TITLE OF ARTICLE:	Susceptibility insensitive single shot MRI combini	
ISSN:	0740-3194	
OTHER NOS/LETTERS:	Library reports holding volume or year 8505245 7760714	
SOURCE:	PubMed	
CALL NUMBER:	W1 MA34IF	
REQUESTER INFO:	JEFFDUYN	
DELIVERY:	E-mail: jhd@helix.nih.gov	
REPLY:	Mail:	

NOTICE: THIS MATERIAL MAY BE PROTECTED BY COPYRIGHT LAW (TITLE 17, U.S. CODE)

---National-Institutes-of-Health,-Bethesda,-MD-----

Susceptibility Insensitive Single Shot MRI Combining BURST and Multiple Spin Echoes

Peter van Gelderen, Chrit T.W. Moonen, Jeff H. Duyn

A single shot MR imaging technique insensitive to magnetic susceptibility effects is introduced. The method allows multi-slice imaging in areas with poor magnetic field homogeneity, and can be implemented on standard clinical scanners. The design is based on the combination of a BURST excitation with multiple RF refocusing pulses. Images were obtained at 1.5 T on phantoms and human brain with a matrix size of 64×54 and a resolution of 4×4 mm in 230 ms.

Key words: MRI, BURST, MSE, GRASE.

INTRODUCTION

Since the inception of MRI, attempts have been made to acquire a complete 2D image in a single excitation. An important advantage over multi-shot imaging is the suppression of the effects of motion on image quality. Single shot imaging has been used extensively in functional neuroimaging, cardiac imaging, and studies of diffusion. Currently, a variety of single shot techniques is available. These techniques either use repeated gradient refocusing (EPI) (1), or repeated RF refocusing (RARE) (2), or a combination of the two (GRASE) (3). Each has distinct advantages and disadvantages. EPI requires fast gradients, currently not available on conventional clinical scanners. Both EPI and GRASE suffer from image artifacts in areas with poor B_0 -homogeneity, related to the switching of polarity of the readout gradient. Single shot RARE requires excellent B_1 -homogeneity, and is limited by restrictions on RF power deposition.

An alternative single shot technique, called BURST has been proposed by Hennig (4) and Hennig and Hodapp (5). This technique is less demanding on gradient speed and B_1 -homogeneity, and has minimal B_1 -related artifacts. Its disadvantage is the poor SNR, severely reducing its potential clinical utility. In the following a novel technique is introduced, which combines elements of BURST and RARE, and allows for single shot imaging without B_0 -related artifacts.

METHODS

Brain scans were performed on normal volunteers using a standard 1.5 T GE/SIGNA clinical scanner (GE Medical

Systems, Milwaukee, WI), equipped with 10 mT/m, actively shielded whole body gradients. A standard quadrature head RF coil was used. The human subject protocol was approved by the intramural review board of the National Institute of Mental Health at NIH.

In the standard BURST excitation a continuous gradient is applied both during a DANTE RF pulse train and during acquisition, which results in excitation of strips throughout the whole volume. To limit the BURST excitation to a single slice, two modifications were used: 1) a selection gradient was added, which was refocused for every RF-pulse; 2) the acquisition gradient was switched off during the RF-pulses. A similar excitation pulse was proposed by Le Roux *et al.* (6). The resulting pulse sequence is given in Fig. 1, combining a slice selective BURST excitation and multi-spin echo acquisition (hence called BASE). The use of both positive and negative selection gradient pulses for excitation allowed for minimal interpulse distance with the available gradient power. This was necessary to achieve the minimal echo time in the MSE sequence. With the combination of BURST and MSE, 54 echo signals were created, to produce a 65×54 image.

The RF part of the excitation pulse contained six RF subpulses each with a sinc-shaped envelope (one sinc lobe). A phase modulation scheme of 0, 60, 180, 0, 240, and 180 degrees was applied to these pulses to improve SNR (7). The flip angle of each RF-pulse was slightly below the calculated maximum of $90^\circ/\sqrt{6}$ (7). In combination with the selection gradient, this resulted in excitation of magnetization within a 10-mm thick axial slice. Spatial pre-encoding was performed by addition of gradient pulses in the phase encode direction. The amplitude of these pulses was designed to create a dephasing corresponding to a shift of a single step in k -space.

The multi-spin echo sequence consisted of nine slice selective refocusing pulses with 26 ms spacing. Crusher gradients were used around the refocusing pulses to suppress unwanted coherences. To reduce sensitivity to CPMG effects, the amplitude of the z-crusher gradient was stepped down linearly (from 8 mT/m to -8 mT/m) over subsequent intervals. The use of phase modulated excitation pulses precluded application of CPMG type refocusing. Within each spin echo, six BURST echoes were created by application of an acquisition-gradient pulse with the same polarity as used in the excitation pulse. The amplitude of this gradient was designed to create an echo spacing equal to the separation of the RF excitation subpulses (2 ms). This resulted in zero susceptibility weighting of all six echoes. Phase encode and rewinder gradients were applied around the BURST echo train. The amplitudes of these pulses were designed to position the center of k -space at the first spin echo,

MRM 33:439-442 (1995)

From the NIH In Vivo NMR Research Center, BEIP, NCCR, National Institutes of Health (P.v.G., C.T.W.M.), and the Laboratory of Diagnostic Radiology Research, OIR, NIH, Bethesda, Maryland (J.H.D.).

Address correspondence to: Jeff H. Duyn, Ph.D., Laboratory of Diagnostic Radiology Research, OIR, NIH, Building 10, Room B1N-256, Bethesda, MD 20892.

Received August 3, 1994; revised November 15, 1994; accepted November 15, 1994.

0740-3194/95 \$3.00

Copyright © 1995 by Williams & Wilkins

All rights of reproduction in any form reserved.

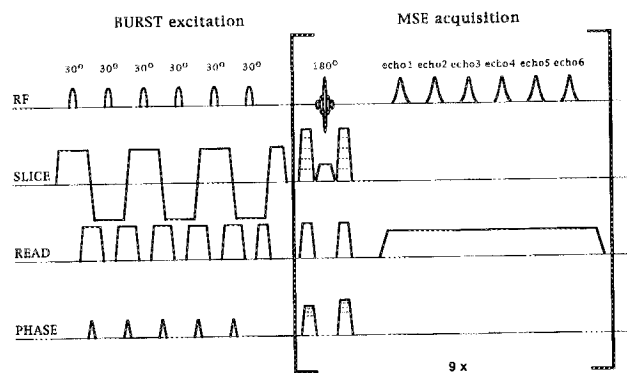


FIG. 1. Pulse diagram of BASE. The method combines a BURST-type excitation with a multi-spin-echo (MSE) acquisition scheme. The part of the diagram enclosed between square brackets is repeated 9 times. The excitation consists of six consecutive RF subpulses in the presence of a slice selection gradient (SLICE). Spatial encoding is incorporated in the BURST excitation by application of gradient pulses in the acquisition (READ) and phase encode (PHASE) directions. The MSE acquisition part employs a series of nine slice-selective refocusing pulses and a gradient pulse in the readout direction to refocus the BURST echo trains. The refocusing pulses are flanked by crusher pulses in all gradient directions to suppress unwanted coherences. Each echo train (echo 1-echo 6) is spatially encoded by gradient pulses in the phase encoding direction (incorporated in the crusher pulses).

whereas higher k -space segments were covered with the later spin echoes (flipping around k -space center on subsequent spin echoes, Fig. 2). The particular encoding scheme was designed for optimal SNR and minimum T_2 -weighting.

Multi-slice imaging was performed by shifting the frequency of both BURST and refocusing RF pulses on

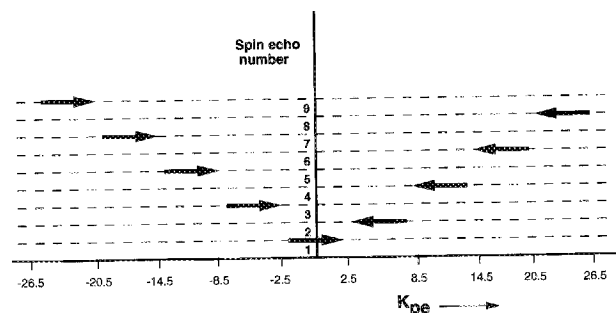


FIG. 2. Phase encoding used in BASE experiment, indicating the order in which k -space lines are scanned. Each BURST echo train scans a segment of the phase-encode dimensions of k -space (k_{pe}). This is indicated with arrows, each spin echo producing one arrow. The direction the arrows indicates the order in which the lines are scanned. The position of the spin echo in the echo train is indicated by the numbering on the vertical axis.

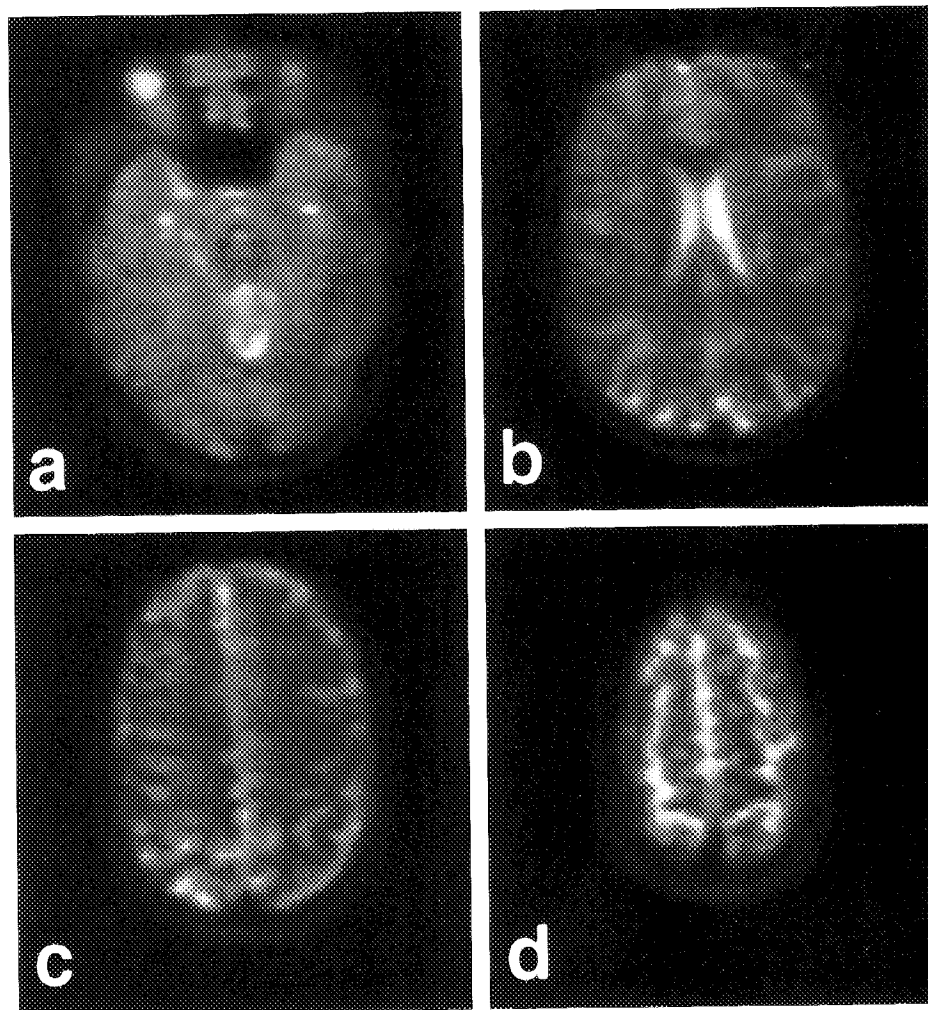


FIG. 3. Four axial slices of normal human brain, obtained with multi-slice BASE experiment, going from inferior (a) to superior (d) in the brain. The repetition time (between slices) was 500 ms. CSF appears bright due to spin-density and T_2 weighting. No shimming was performed on this subject. Note the correct localization of anatomical features, even in the presence of susceptibility affected regions (frontal part of bottom slice).

subsequent repetitions. Due to the alternation of the slice select gradient in the BURST excitation, frequency shifts were inverted on odd numbered burst RF-subpulses (negative selection gradient). For each slice, a 64×54 data matrix was collected using a 24×20 cm field of view (FOV). The total measurement time was 234 ms, repetition time for each slice (TR) was varied between 300 and 6000 ms.

For comparison, single-shot GRASE imaging was performed using five gradient echoes and nine spin echoes, and with a similar k -space scanning strategy; total acquisition time was 210 ms. This was done on a single slice, on which some minor first order shimming was performed. A reference scan with phase encoding gradients switched off was acquired separately to allow for post-acquisition correction for off-resonance effects in the acquisition direction.

Data processing was performed off-line on Sun-SPARC workstations (Sun Microsystems, Mountainview, CA) using IDL processing software (Research Systems, Boulder, CO). After reordering the spin echo signals, the phase of the signals in odd-numbered spin-echo intervals was flipped (with respect to the 180 pulse phase), and the order of the BURST echoes in the even-numbered intervals was reverted. Furthermore, on all BURST echo signals, a phase correction was performed to account for the additional phases induced by the phase modulation of the BURST excitation pulses. Subsequently, after cosine-bell apodization of the data (over 50% of higher k -space points), 2D Fourier transformation was performed, and images were created from magnitude data. The resulting effective resolution in the images was 4×4 mm. For the GRASE data, additional phase correction was performed before FT in the phase encode direction, using estimates of susceptibility induced phase errors, derived from the reference scan (without phase encoding).

RESULTS AND DISCUSSION

An example of a BASE multislice study is given in Figs. 3a–3d. Four slices are displayed from a five-slice study, using a TR of 2500 ms. Slice thickness and interslice gap were both 10 mm. The SNR (average brain signal intensity divided by background intensity in acquisition direction) was in the range of 100–120. Clearly recognizable in these images is CSF, consistent with the substantial T_2 weighting of the BASE sequence. (e.g., in the ventricular spaces in Fig. 3b, and most clearly in the sulci of the superior part of the brain, i.e., slice d) (Fig. 3d). Also apparent in these images is the preserved image quality in areas of poor B_0 -homogeneity, such as in the anterior part of slice a (Fig. 3a). The studies of normal brain consistently showed good image quality, and proved insensitive to B_0 -shim and resonance frequency (misadjustments). This is in contrast with images obtained with GRASE or EPI, which often exhibit ghosting artifacts. Figure 4 gives a view of the background signal by the use of a 20-fold blown-up intensity scale. No distinct ghost artifacts are observed, demonstrating the insensitivity to susceptibility-related artifacts. This em-

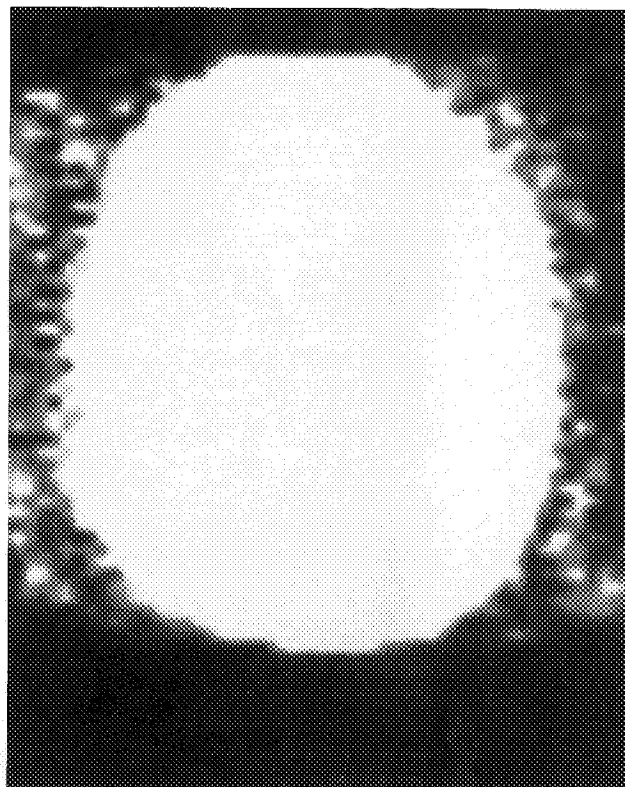


FIG. 4. Ghosting artifacts observed in BASE-image. The image intensity of Fig. 3c was multiplied 20-fold. Note the absence of distinct ghost images, even from the lipid regions. Some smearing is observed in the phase-encode direction (running left to right in the image), attributed to T_2 -related signal decay over the echoes.

phasizes the flexibility of BASE with respect to artifact-free coverage of the entire brain, despite the unavoidable regional differences in resonance frequency.

The studies with variation of TR did not show significant changes in image quality. The studies with delay time between slices of less than 1000 ms showed some overall signal loss in specific slices, related to saturation effects in combination with interference between slices. This is attributed to the relatively poor slice profiles selected by the BASE-sequence.

Figure 5 shows a comparison of images obtained with single-shot GRASE (as described in the method section) and a BASE image from the same slice. Although the GRASE image shows a 1.5 times better SNR, it is clearly more sensitive to susceptibility and off-resonance related distortions, which are most clearly recognized as ghost images. The lower SNR of the BASE images is explained by the expected signal loss due to the BURST excitation ($1/\sqrt{6}$) combined with a $\sqrt{2}$ reduction of the noise due a twofold reduction of the acquisition bandwidth.

Repeated application of the sequence ($TR = 1500$ ms) demonstrated an image stability in most areas of the brain of 1.5%, except for the ventricular spaces, which in some of the images caused a distinct ghost. We tentatively attribute the effect to pulsatile CSF flow. The phase modulated BURST excitation results in strips of transverse magnetization with large phase differences. The

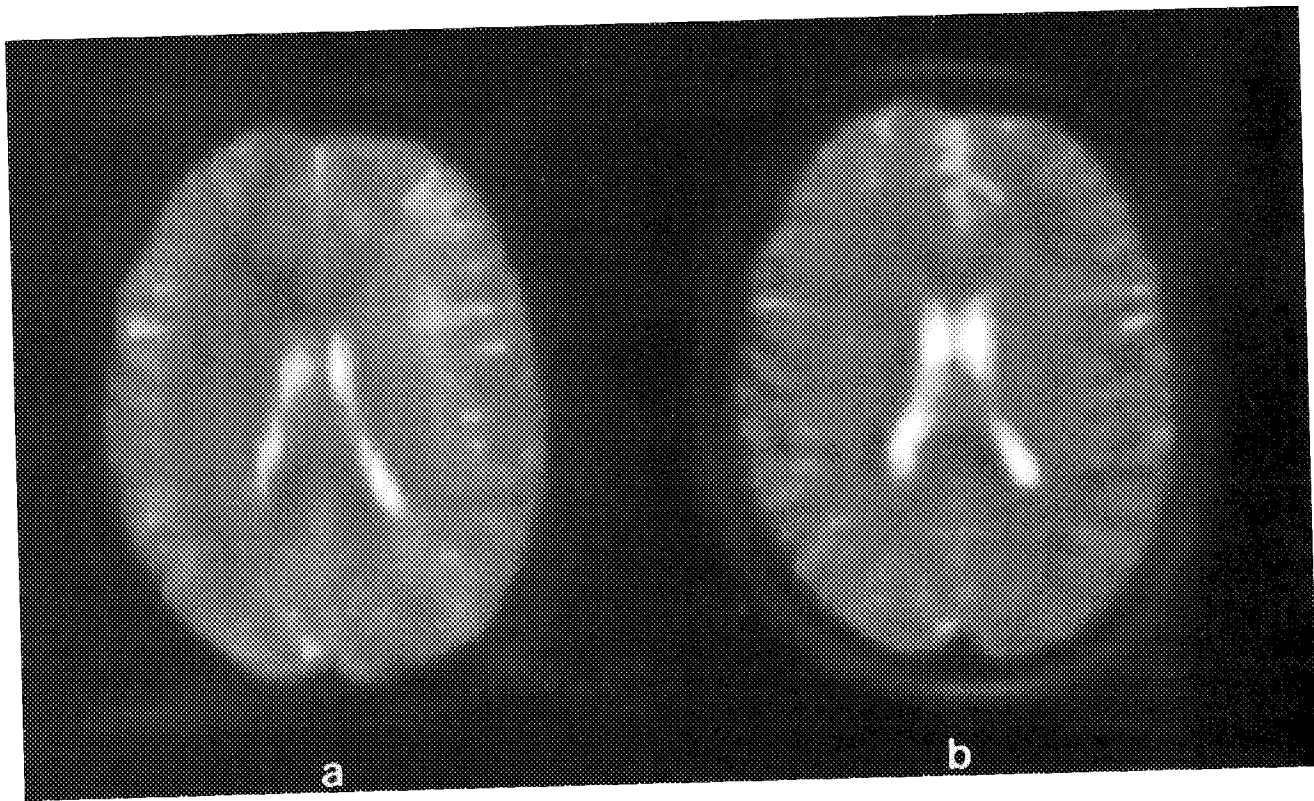


FIG. 5. Comparison between BASE (b) and single shot GRASE (a). Although the images were acquired under similar conditions, the BASE image shows superior image quality. The GRASE image clearly shows localization errors for scalp-lipids related to off-resonance effects, an artifact not seen in the BASE image.

strips have a width of approximately 0.6 mm. Motion during the acquisition on this scale leads to a decrease in echo amplitude and phase deviations. This problem could be alleviated by the use of gating or inversion nulling of CSF.

CONCLUSION

A novel single shot imaging method has been introduced and successfully applied to imaging of human brain on a standard clinical scanner. As compared with existing single shot methods, the method shows reduction of image artifacts, but a somewhat lower SNR. The method does not require the acquisition of a separate reference scan, and allows imaging in regions with poor magnetic field homogeneity due to susceptibility effects. These characteristics make it an excellent candidate for application to diffusion imaging. Its insensitivity to off-resonance effects also makes it a good candidate for imaging areas with high fat concentrations.

ACKNOWLEDGMENTS

The authors thank Dr. G. Liu for her assistance with implementation of the multi-spin echo sequence, and Drs. J. A. Frank and N. Ramsey for their helpful suggestions and support.

REFERENCES

1. P. Mansfield, I. Pykett, Biological and medical imaging by NMR. *J. Magn. Reson.* **29**, 355-373 (1978).
2. J. Hennig, A. Nauerth, H. Friedburg, RARE imaging: a fast imaging method for clinical MR. *Magn. Reson. Med.* **3**, 823-833 (1986).
3. K. Oshio, D. A. Feinberg, Single-shot GRASE imaging without fast gradients. *Magn. Reson. Med.* **26**, 355-360 (1992).
4. J. Hennig, Fast imaging using BURST excitation pulses, in "Proc., SMRM, 7th Annual Meeting, 1988," p. 238.
5. J. Hennig, M. Hodapp, Burst imaging. *Magma* **1**, 39-48 (1993).
6. P. Le Roux, J. Pauly, A. Macovski, BURST excitation pulses, in "Proc., SMRM, 10th Annual Meeting, 1991," p. 269.
7. P. van Gelderen, J. H. Duyn, C. T. W. Moonen, Analytical solution for phase modulation in BURST imaging. *J. Magn. Reson.*, in press.

Multi-Shot EPI for Improvement of Myocardial Tag Contrast: Comparison with Segmented SPGR

Chao Tang, Elliot R. McVeigh, Elias A. Zerhouni

To assess the potential value of multi-shot EPI relative to segmented k -space SPGR for myocardial tagging, we measured tag contrast for both sequences in a phantom and human study and compared it with theoretical predictions. In the human heart, EPI tag contrast was three times that of SPGR at the end of systole. Tag duration was lengthened with EPI to at least 600 ms. In addition, the entire heart was examined in a total of 32 heartbeats with EPI versus 152 heartbeats with SPGR.

Key words: magnetic resonance imaging; EPI; SPGR; myocardial tagging.

INTRODUCTION

Myocardial tagging techniques can provide unique measurements of myocardial deformation (1-4). Because of misregistration caused by breathing, emphasis has recently been placed on the development of single breath-hold pulse sequences capable of acquiring multiple phases of the cardiac cycle in a reduced number of heartbeats. Segmented k -space tagged SPGR sequences have gained acceptance and can be implemented on standard hardware (5, 6). These sequences, however, suffer from a poor signal-to-noise ratio and significant tag fading by end-systole. Furthermore, only one slice per breath-hold can be acquired with tagged SPGR. Echo-planar imaging (EPI) (7-9) is a method that provides not only the potential for imaging the entire heart in a single breath-hold, but also higher signal-to-noise ratio and tag/tissue contrast. A recently installed EPI system enabled us to explore EPI myocardial tagging. In this study, we compared the tag contrast in SPGR and EPI images.

METHODS AND THEORY

Pulse Sequence

Figures 1a and 1b show the SPGR and EPI tagging pulse sequences, respectively. Parallel tags were used in a direction perpendicular to the readout direction, which had higher spatial resolution than the phase encoding

direction. Magnetization in the tagged regions was inverted to maximize the persistence of tag lines. The tagging pulse was ECG-triggered and followed by multiple RF excitations. For any one slice, multi-phase images were captured in a single breath-hold. For any one phase, multiple phase encoding views were acquired in the same R-R interval. The views were interleaved to reduce ghost artifacts due to signal modulation in the phase encoding direction (5, 6, 10). In SPGR, a truncated RF excitation pulse and partial readout were used to reduce the echo time (TE) and the repetition time (TR), so that motion artifacts were minimized and high temporal resolution images were obtained. The phase cycling method (11) was used to spoil the nonprimary echoes. In EPI, the slices were interleaved such that each slice was excited only once per cardiac cycle. The effective repetition time was the length of the cardiac cycle. The effective repetition time was the length of the cardiac cycle. A spectral-spatial selective pulse (12) that excited water only was used to reduce chemical shift artifact.

Theory

In SPGR, a slice is excited repeatedly. The longitudinal magnetization just before the n th RF pulse can be expressed as

$$M_z(n) = 1 + [M_z(n-1)\cos\alpha - 1]e^{-TR/T_1} \quad [1]$$

where T_1 is the spin-lattice relaxation time, TR is the repetition time, α is the flip angle, and M_0 is defined as 1. The difference in longitudinal magnetization of spins in nontagged and tagged regions is

$$\Delta M_z(n) = \Delta M_z(n-1)\cos\alpha e^{-TR/T_1} \quad [2]$$

Using this relation recursively, the tag contrast at the n th RF pulse can be expressed as a function of the tag contrast at the first time frame, $\Delta M_z(1)$, which is

$$\Delta M_z(n) = \Delta M_z(1)\cos^{n-1}\alpha e^{-(n-1)TR/T_1} \quad [3]$$

Because magnetization in the tagged regions is inverted after each ECG trigger, magnetization in the tagged regions takes longer to reach a steady state than in nontagged regions. The approach to steady state is very dependent on the imaging flip angle used. As the spins in both regions are driven to equilibrium in an SPGR sequence, the available M_z prior to the next tagging pulse is much smaller. Subsequently, the zero crossing of the inverted magnetization is advanced, leading to less persistence of the tags. In our experimental conditions, the difference of magnetization in both regions in the beginning of R wave is very small because of the multiple excitation pulses in the same physical location and the relatively long recovery time after the last RF pulse. This is demonstrated by the low tag contrast in the end sys-

MRM 33:443-447 (1995)

From the Department of Biomedical Engineering (C.T., E.R.M.) and the Department of Radiology (E.R.M., E.A.Z.), The Johns Hopkins University School of Medicine, Baltimore, Maryland.

Address correspondence to: Elliot McVeigh, Ph.D., Medical Imaging Laboratory, Departments of Biomedical Engineering and Radiology, 407 Traylor Building, 720 Rutland Avenue, The Johns Hopkins University School of Medicine, Baltimore, MD 21205.

Received July 20, 1994; revised November 16, 1994; accepted November 17, 1994.

This research was supported by the National Institutes of Health grants HL45683 and HL45090. Chao Tang was supported by a fellowship from the Whitaker Foundation.

0740-3194/95 \$3.00

Copyright © 1995 by Williams & Wilkins

All rights of reproduction in any form reserved.

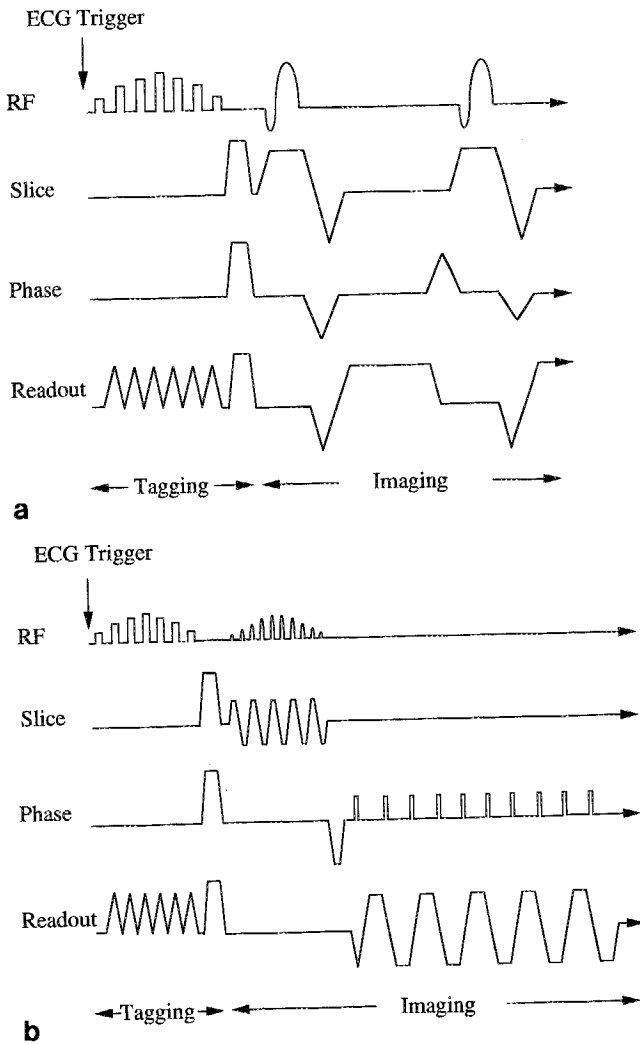


FIG. 1. The SPGR and EPI pulse sequences are shown in (a) and (b), respectively. The tagging pulse is ECG-triggered and is followed by multiple imaging pulses. The tag lines are placed perpendicular to the readout direction. The SPGR sequence is made as short as possible. A spectral-spatial excitation RF pulse is used in EPI to reduce chemical shift artifacts.

tolic images. If we can assume that magnetization in both tagged and nontagged regions has reached a steady state at the end of data acquisition in each cardiac cycle, the tag contrast at the first time frame is

$$\Delta M_z(1) = 2 \left(1 - \frac{1 - \cos \alpha}{1 - \cos \alpha e^{-TR/T_1}} e^{-(T-(N-2)TR)/T_1} \right) \quad [4]$$

where N is the total number of RF pulses applied in each cardiac cycle and T is the length of a cardiac cycle. Therefore, the tagging contrast of SPGR images after the n th RF pulse is

$$C_{\text{spgr}}(n) = 2 \left(1 - \frac{1 - \cos \alpha}{1 - \cos \alpha e^{-TR/T_1}} e^{-(T-(N-2)TR)/T_1} \right) \cdot \cos^{n-1} \alpha e^{-(n-1)TR/T_1} \sin \alpha e^{-TE/T_2^*} \quad [5]$$

where TE is the echo time, and T_2^* is the effective spin-spin relaxation time. The error in estimating the initial tag contrast will only shift the tag contrast curve up and

down, but will not change the shape of the curve. In the results shown later, the theoretical curve was normalized to the first experimental data point.

For multi-slice and multi-phase EPI cardiac imaging, magnetization is not affected by the tagging pulse in the nontagged regions. The longitudinal magnetization in the nontagged regions of myocardium is independent of time delay after the ECG trigger; it is only dependent on flip angle and T , which is equal to the length of a cardiac cycle. If a 90° pulse is used for imaging, the longitudinal magnetization of nontagged regions at any time, t , after the tagging pulse and just before the imaging RF pulse is

$$M_z(t) = 1 - e^{-t/T_1} \quad [6]$$

In the tagged regions, the spin magnetization is inverted by the tagging pulse at each QRS. Because the time from the tagging pulse to the imaging pulse is different for each phase, the signal intensity in the tagged regions is different for each phase, and the tags fade with time. The longitudinal magnetization in tagged regions at time t after the tagging pulse is

$$M_z(t) = 1 - 2e^{-t/T_1} + e^{-t/T_1} \quad [7]$$

The tag contrast between the tagged and nontagged regions is

$$C_{\text{epi}}(t) = 2(e^{-t/T_1} - e^{-t/T_1})e^{-TE/T_2^*} \quad [8]$$

Experiments

All the data were acquired on a GE 1.5 Tesla Signa system (Milwaukee, WI) equipped with a prototype GE single axis SR-230 echo-planar system. This EPI system can switch its fastest gradient from 0 to 2.3 Gauss/cm in $100 \mu\text{s}$. Because only a single fast gradient was available, all EPI images were acquired in the axial plane. The SPGR images were also acquired in the axial plane to ensure an equal comparison.

A stationary phantom made of copper sulfate ($T_1 = 800$ ms, $T_2 = 500$ ms) was used to emulate the spin-lattice relaxation rate of the myocardium. This phantom study was designed to validate the tag contrast predicted by Eqs. [5] and [8]. The head coil was used for both EPI and SPGR imaging. The phase encoding steps were chosen so that the spatial resolution was the same in both SPGR and EPI images. The pulse was triggered at every 1000 ms. In SPGR, 60 phases, which were used to demonstrate the signal evolution of tagged and nontagged regions, and eight slices were acquired. The FOV was 30 cm, voxel size was $1.2 \times 3.3 \times 10$ mm. The repetition time, TR , was 6.5 ms, the echo time, TE , was 2.3 ms, and one average was used. An flip angle of 11° was chosen to optimize the tag contrast (10). Fractional readout was used to shorten the echo time. In the readout direction, 160 points were acquired and half Fourier reconstruction was used to obtain 256 point image resolution. The readout bandwidth was 64 kHz. In the phase encoding direction, the number of phase encoding steps were 90 and zero padding was applied for the remaining 166 views. One view was acquired for each phase in each cardiac cycle, so that the temporal resolution was 6.5 ms. In EPI, eight slices and eight phases were acquired with a temporal resolu-

tion of 37 ms. Voxel size was $1.2 \times 3.3 \times 10$ mm. The repetition time, TR , was 1000 ms, the echo time, TE , was 13 ms, and flip angle was 90° . Rectangular FOV was used. Ten views were acquired for each phase in each cardiac cycle. All the data for each phase were obtained in four cardiac cycles. The temporal resolution was 37 ms. In the readout direction, 256 points of data were acquired and FOV was 30 cm. The readout bandwidth was 250 kHz. In the phase encoding direction, FOV was 21 cm, 40 phase encoding steps were used, and half Fourier reconstruction was used to obtain 64 point image resolution. Echo shifting was used in EPI to eliminate artifacts along the phase encoding direction. In both EPI and SPGR, a 24-pixel tag width and an 84-pixel tag separation were used to sample tag contrast accurately. The flip angle of spins in tagged regions was 180° , the duration of the tagging pulses was 18 ms, and the tagging gradient area between two RF pulses was 24 Gauss $\mu\text{s}/\text{cm}$. The tag contrast was measured by subtracting the minimum from maximum magnitude value along a line perpendicular to the tag lines after correcting for the sign of the tag for those time frames that preceded the zero crossing of tagged spins.

In a human volunteer study, the parameters were the same as those used in the phantom study unless noted otherwise. The body coil was used in both EPI and SPGR imaging. The tag shape was narrowed to a two-pixel tag width and a seven-pixel tag separation. In SPGR, images of eight slices and twelve phases were acquired in eight breath-holds; each breath-hold lasted 19 heartbeats, where the first heartbeat was used to stabilize the magnetization and no data were acquired. Five views were acquired for each phase in each cardiac cycle, so that the temporal resolution was 32.5 ms. In EPI, images of 8 slices and 8 phases were acquired in a single breath-hold lasting 32 heartbeats. The temporal resolution was 37 ms.

RESULTS

The experimentally measured and theoretically predicted contrast between tagged and nontagged regions in the phantom is plotted in Fig. 2. There is good agreement between the theoretical and experimental data. Fig. 3 shows the theoretical prediction of tag contrast when T_2^* is 20 ms, which is close to the expected T_2^* of myocardium. In Fig. 3, the tag contrast in EPI is higher at all times than in SPGR. In particular, the contrast in EPI is 100% and 260% higher than in SPGR at 60 and 330 ms after the ECG trigger, respectively. The tag contrast-to-noise ratio of EPI images at 600 ms is equal to the contrast of SPGR images at 200 ms; the tag lines of routine SPGR images can be easily visualized at this delay time.

Figure 4 shows representative images acquired from a normal volunteer at 60 and 330 ms after the ECG trigger using SPGR and EPI techniques, respectively. The tag contrast-to-noise in the echo-planar images is clearly better than in SPGR and is plotted in Fig. 5. The tag contrast-to-noise in EPI is 70% and 200% higher than in SPGR at 60 and 330 ms after the ECG trigger, respectively. The results are in good agreement with that in Fig. 3. The difference in Figs. 3 and 5 may be caused by the narrow tag lines and motion in the human study.

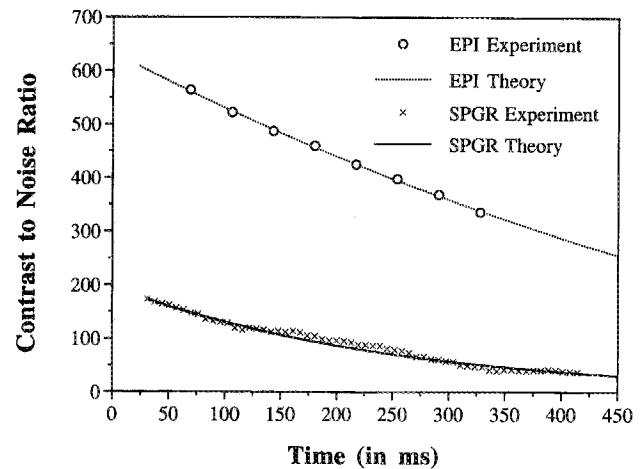


FIG. 2. The tag contrast in SPGR and EPI images as a function of time after the ECG trigger. The solid and dotted lines represent the theoretical predictions of SPGR and EPI tag contrast, respectively. The crosses and circles represent the tag contrasts of SPGR and EPI images, respectively.

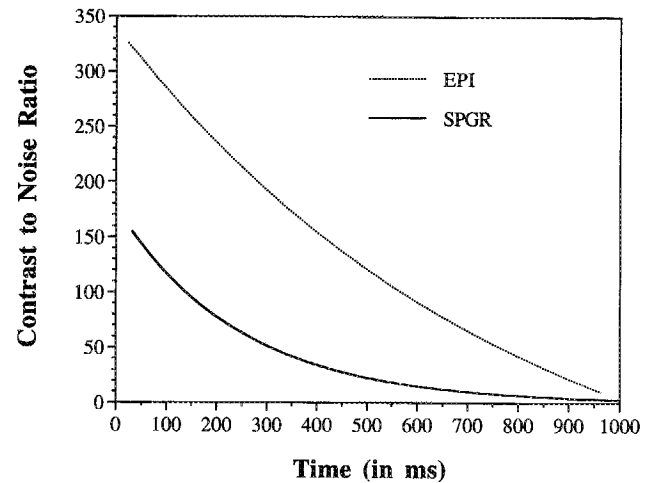


FIG. 3. The tag contrast in SPGR and EPI images when T_2^* is 20 ms. The solid and dotted lines represent the theoretical predictions of SPGR and EPI tag contrast, respectively. The tag contrast of EPI images is 100% and 260% higher than that in SPGR images in 30 and 330 ms after the ECG trigger, respectively. The tag contrast of EPI image in 600 ms after ECG trigger is approximately equal to the contrast of SPGR image in 200 ms after ECG trigger.

DISCUSSION AND CONCLUSIONS

As demonstrated in Figs. 2 and 5, not only is the tag contrast-to-noise ratio in EPI images much higher than in SPGR images but tags persist longer in EPI images. EPI is likely to be used to assess myocardial motion further into diastole since EPI contrast at 600 ms is equal to SPGR contrast at 200 ms. In EPI, slices are interleaved and each slice is excited only once in each cardiac cycle. The decrease of tag contrast in later cardiac phases is caused only by the spin-lattice relaxation as shown in Eq. [8]. In SPGR, a slice is excited many times in each cardiac cycle. During each excitation, a fraction of magnetization in both tagged and nontagged regions is brought into the transverse plane, reducing the tag contrast. The decrease of tag contrast is caused not only by the spin-lattice relaxation but also by the saturation effects of RF pulses

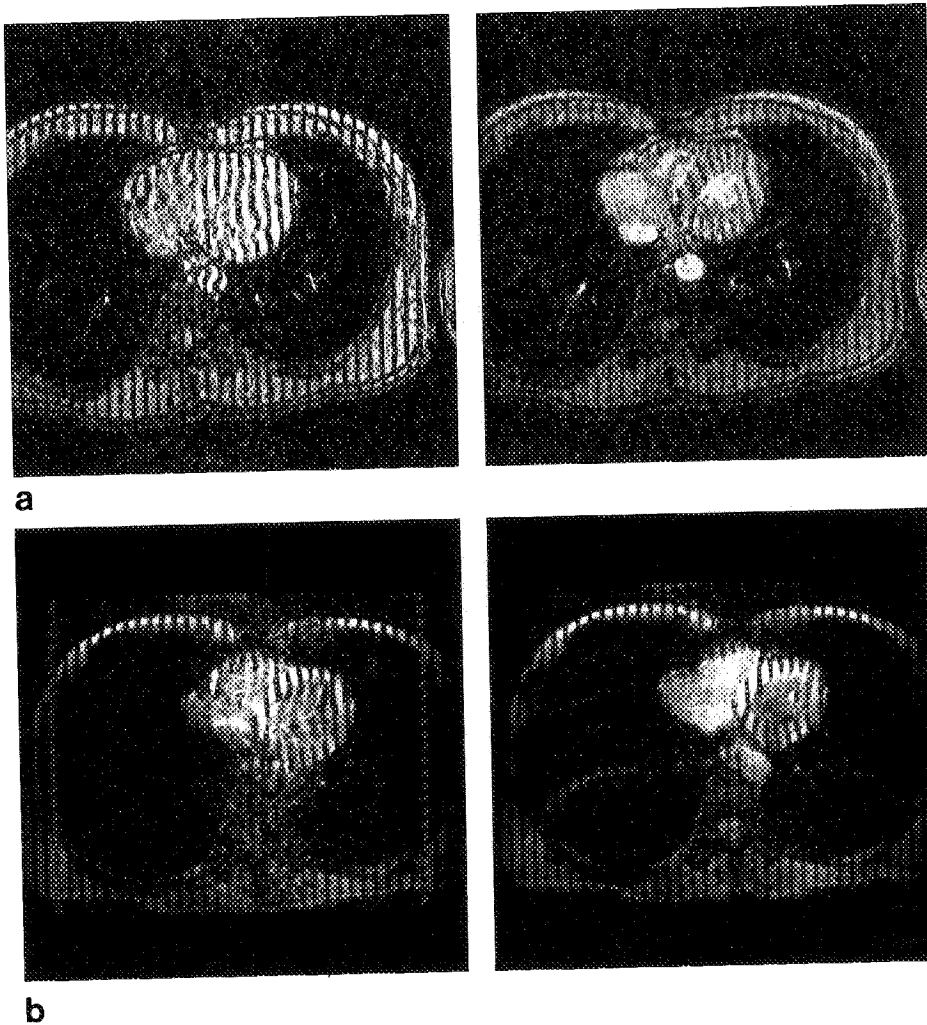


FIG. 4. Comparison of tag contrast with SPGR (a) and EPI (b) images. The left column shows images acquired 30 ms after the ECG trigger. The right column shows the same slice acquired at 330 ms after the ECG trigger.

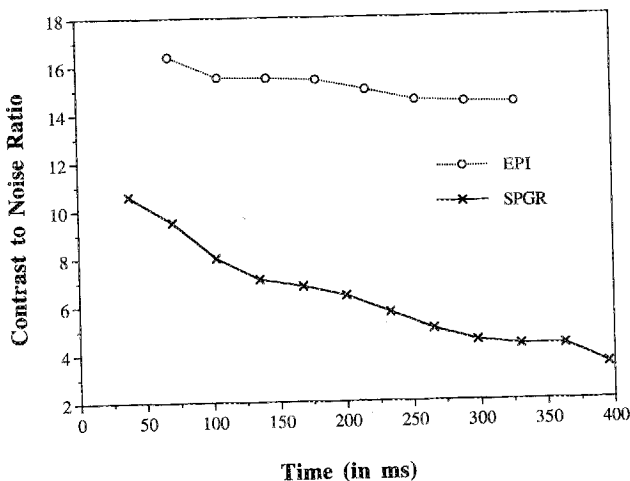


FIG. 5. The tag contrast of myocardium measured in the series of SPGR and EPI images shown in Fig. 4. The tag contrast of EPI images is about 70% and 200% higher than SPGR images at 30 and 330 ms after the ECG trigger, respectively.

as shown in the exponential and cosine terms of Eq. [5]. If a large flip angle is used, the tag contrast will disappear quickly because of the saturation effect. If a small flip angle is used, the saturation effect is minimized and the decrease of tag contrast is dominated by spin-lattice relaxation. To increase the persistence of tag contrast, an

optimal flip angle (10), typically around 10° – 20° , or variable flip angles (13), can be used.

The total imaging time for a stack of multi-phasic images with EPI is 32 heartbeats and a single breath-hold. This is much shorter than the imaging time required by SPGR, which takes 152 heartbeats and eight breath-holds. Because all of the EPI images are obtained in a single breath-hold, the respiratory motion and registration artifacts that result from multiple breath-holds are eliminated. If a patient cannot manage a breath-hold for 32 heartbeats, two 16 heartbeat breath-holds can be used, but the advantage of a single breath-hold is lost. SPGR images are very robust to chemical shift artifacts and short T_2^* values. This cannot be said for EPI acquisitions, which require more careful tuning.

The temporal resolution of segmented k -space SPGR depends on the number of phase encode views per movie frame. It is clear that using the fast gradients will improve either the time resolution or the SNR of the segmented k -space images by reducing the time required to play out the "dead-time" pulses such as the phase encode pulse and the slice rewinder. If the fast gradients are used, either the temporal resolution can increase approximately 25% when the readout bandwidth is fixed, or the tag CNR can increase approximately 40% by using the optimal bandwidth when the temporal resolution is fixed (14).

In conclusion, EPI can acquire the same amount of myocardial tagging data in a shorter time than SPGR. The tag contrast in EPI is much higher than in SPGR and permits tag visualization much further into diastole.

ACKNOWLEDGMENTS

The authors thank Ergin Atalar for assistance with the segmented k -space SPGR pulse sequence.

REFERENCES

1. E. A. Zerhouni, D. M. Parish, W. J. Rogers, A. Yang, E. P. Shapiro, Human heart: tagging with MR imaging—method for noninvasive assessment of myocardial motion. *Radiology* **169**, 59, (1988).
2. L. Axel, L. Dougherty, MR imaging of motion with spatial modulation of magnetization. *Radiology* **171**, 841–849 (1989).
3. A. A. Young, L. Axel, L. Dougherty, D. K. Bogen, C. S. Parenteau, Validation of tagging with MR imaging to estimate material deformation. *Radiology* **188**(1), 101–108 (1993).
4. C. C. Moore, S. B. Reeder, E. R. McVeigh, Tagged MR imaging in a deforming phantom: photographic validation. *Radiology* **190**, 765–769 (1994).
5. D. J. Atkinson, R. R. Edelman, Cineangiography of the heart in a single breath hold with a segmented turbo FLASH sequence. *Radiology* **178**, 357–360 (1991).
6. E. R. McVeigh, E. Atalar, Cardiac tagging with breath hold CINE MRI. *Magn. Reson. Med.* **28**, 318–327 (1992).
7. P. Mansfield, I. L. Pykett, Biological and medical imaging by NMR. *J. Magn. Reson.* **29**, 355–373 (1978).
8. G. C. McKinnon, Ultrafast interleaved gradient-echo-planar imaging on a standard scanner. *Magn. Reson. Med.* **30**(5), 609–616 (1993).
9. D. R. Wetter, J. F. Debatin, G. C. McKinnon, J. A. Boner, Interleaved echo-planar imaging of the heart, in "Proc., SMR, 1st Annual Meeting, 1993," p. 139.
10. S. B. Reeder, E. R. McVeigh, Tag contrast in breathhold CINE cardiac MRI. *Magn. Reson. Med.* **31**, 512–525 (1994).
11. A. P. Crawley, M. L. Wood, R. M. Henkelman, Elimination of transverse coherence in FLASH MRI. *Magn. Reson. Med.* **8**, 248–260 (1988).
12. C. H. Meyer, J. M. Pauly, A. Macovski, D. G. Nishimura, Simultaneous spatial and spectral selective excitation. *Magn. Reson. Med.* **15**(2), 287–304 (1990).
13. S. J. Wang, D. G. Nishimura, A. Macovski, Multiple-readout selective inversion recovery angiography. *Magn. Reson. Med.* **17**(1), 244–251 (1991).
14. S. B. Reeder, E. R. McVeigh, The Effect of high performance gradients on fast gradient echo imaging. *Magn. Reson. Med.* **32**, 612–621 (1994).